

This is a postprint version of the following published document:

Sádaba, S., Herráez, M., Naya, F., González, C., Llorca, J. & Lopes, C. (2019). Special-purpose elements to impose Periodic Boundary Conditions for multiscale computational homogenization of composite materials with the explicit Finite Element Method. *Composite Structures*, 208, 434–441.

DOI: [10.1016/j.compstruct.2018.10.037](https://doi.org/10.1016/j.compstruct.2018.10.037)

© 2018 Elsevier Ltd. All rights reserved.



This work is licensed under a [Creative Commons Attribution-NonCommercial-NoDerivatives 4.0 International License](https://creativecommons.org/licenses/by-nc-nd/4.0/).

Special-purpose elements to impose Periodic Boundary Conditions for computational homogenization using explicit FE

S. Sádaba¹, M. Herráez^{1,2}, F. Naya^{1,2}, C. González^{1,2}, J. Llorca^{1,2},
C.S. Lopes^{1*}

¹*IMDEA Materials, C/Eric Kandel 2, 28906 - Getafe, Madrid, Spain*

²*Department of Materials Science, Polytechnic University of Madrid, E.T.S. de Ingenieros de Caminos, 28040 Madrid, Spain*

Abstract

A novel methodology to introduce Periodic Boundary Conditions (PBC) on periodic Representative Volume Elements (RVE) in Finite Element (FE) solvers with dynamic explicit time integration is presented. This implementation aims at overcoming the difficulties of the explicit FE method in dealing with standard PBC. The proposed approach is based on the implementation of a user-defined element, named a Periodic Boundary Condition Element (PBCE), that enforces the periodicity between periodic nodes through a spring-mass-dashpot system. The methodology is demonstrated in the multiscale simulation of composite materials. Two showcases are presented: one at the scale of computational micromechanics, and another one at the level of computational mesomechanics. The first case demonstrates that the proposed PBCE allows the homogenization of composite ply properties through the explicit FE integration approach with similar reliability to the equivalent implicit simulations with traditional PBC. The second case demonstrates that the PBCE can be applied to the computational technique of Periodic Laminate Elements (PLE) to homogenize elastic and strength properties of entire laminates. Both demonstrations strongly support the method for the application of multiscale virtual testing to the building-block certification of composite materials.

*Corresponding author: claudiosaul.lopes@imdea.org

Keywords: Explicit FEM, Periodic Boundary Conditions (PBC), Homogenization, Multiscale computational mechanics, Composite materials

1. Introduction

The use of Representative Volume Elements (RVE) has become a very popular numerical approach for the purpose of homogenization in highly heterogeneous materials. This technique allows the reproduction of uniform stress states in a domain and thus, the prediction of the homogenized thermo-mechanical properties including elasticity and strength. Apart from the selection of the RVE size, which must be sufficient to capture the stress-strain response and failure mechanisms of the composite, the applied boundary conditions play a key role on the assessment of the homogenized properties. There are three common types of boundary conditions: uniform boundary displacements or isostrain (Hill-Reuss), uniform boundary tractions or isostress (Hill-Voigt) and Periodic Boundary Conditions (PBC). The use of PBC on the RVE boundaries implies that smaller analysis domains are sufficient to obtain reliable homogenized properties [1]. Due to this reason, PBCs have been extensively employed in computational homogenization.

The classical approach to introduce PBC in a RVE is by means of the definition of strong relations (equations) between periodic nodes, hence imposing constraints to their allowed displacements. In its essence, this method requires the mesh to be periodic, in such a way that every node on each RVE boundary has its homologous node on the respective opposite (periodic) boundary, although enhancements, based on polynomial interpolation [2, 3] and Lagrange multipliers [4], have been proposed in order to avoid the need of matching the mesh topology on opposite RVE boundaries. Either way, the traditional PBC approach is generally appropriate for implicit integration numerical schemes. In dynamic explicit time integration solvers, however, the fulfilment of the periodicity equations leads to spurious displacement oscillations that often invalidate the numerical solution. To overcome this issue, this work proposes the imposition of PBC in explicit FE solvers through special-purpose elements, named *Periodic Boundary Condition Elements* (PBCE). This approach is specially well suited for multiscale computational analyses of composite materials.

With the advances in computing power and the growing costs associated to physical experiments for certification of composites, multiscale virtual testing based on the Finite Element Method (FEM) has become a popular tool

35 in the characterization and evaluation of composite materials and structures
36 [5]. This approach often requires homogenization techniques, as the physical
37 response of composite materials at the macroscale is a direct consequence of
38 their microstructural features and architecture. Moreover, the behaviour of
39 the composite might depend on microstructural features other than the prop-
40 erties and topology of the microconstituents (fibres, matrix and interfaces),
41 such as fibre volume fraction, fibre size and shape distributions, distance
42 between neighbouring fibres, voids, among others. Computational homoge-
43 nization techniques are ideal tools to take all these effects into account.

44 The elastic, plastic and fracture responses of laminated Fibre Reinforced
45 Polymers (FRP) at the macroscale can be computed efficiently by following
46 a stepwise bottom-up multiscale approach [5–7]. In the first step, *compu-*
47 *tational micromechanics* is employed to predict the homogenized behaviour
48 of a unidirectional fibre-reinforced yarn or ply, in 2D (e.g. [8–11]) or 3D
49 spaces (e.g. [12–15]), with input properties resulting from the experimental
50 characterization of the composite microconstituents: fibre [16], matrix [11]
51 and fibre/matrix interface [17]. In the case of ply architectures with higher
52 complexity than unidirectional fibres, such as in textile composites, a subse-
53 quent homogenization step needs to be performed based on the previously
54 computed behaviour of the unidirectional yarns, the response of the bulk
55 resin matrix and on the topology of the Representative Unit Cell (RUC) of
56 the fabric (e.g. [18–21]). From the orthotropic ply behaviour and lamina ori-
57 entations within a ply stacking, *computational mesomechanics* can be used
58 to predict the behaviour of the laminate (e.g. [22–24]). At this step, the
59 response of the discrete ply interfaces also needs to be taken into account,
60 as laminated FRP are prone to delamination. The homogenized behaviour
61 of the laminate can then be applied to the design of composite laminated
62 structures, by employing *computational structural mechanics* [5–7].

63 Some of the aforementioned modelling techniques impose severe non-
64 linearities to the respective numerical problems which become intractable
65 by implicit integration FE solvers. In such cases, explicit numerical schemes
66 become the only viable alternative to achieve meaningful results. Hence, the
67 PBCE approach proposed in this paper constitutes an enabling technology
68 for multiscale computational homogenization in composite materials.

69 The formulation of the PBCE for general 3D FE problems and its imple-
70 mentation as a user-defined element in Abaqus/Explicit [25] are detailed in
71 section 2. The reliability and applicability of the approach are then demon-
72 strated in the framework of multiscale computational analysis of composites,

73 in section 3. First, the PBCE method in combination with RVE is applied to
74 micromechanical homogenization of unidirectional FRP yarns or plies. The
75 results are evaluated through the correlation of numerical results obtained
76 with traditional PBC and new PBCE. Then, PBCE in combination with
77 Representative Laminate Elements (RLE) are proposed for the homogeniza-
78 tion of laminate behaviour through computational mesomechanics. Finally,
79 the concluding remarks are drawn in section 4.

80 2. Definition of the Periodic Boundary Element

81 Periodic boundary conditions guarantee the periodicity of the mechanical
82 fields and ensure the continuity with the neighboring RVE as a jigsaw puzzle.
83 These boundary conditions are set by enforcing that the difference between
84 displacement vectors, \mathbf{u} , of opposite sides of an RVE of lengths $\ell_1 \times \ell_2 \times \ell_3$
85 is equal to an imposed relative displacement, \mathbf{U}_i , that is:

$$\begin{aligned} \varphi_1(x_2, x_3, \mathbf{U}_1) &= (\mathbf{u}(0, x_2, x_3) - \mathbf{u}(\ell_1, x_2, x_3)) - \mathbf{U}_1 = \mathbf{0} \\ \varphi_2(x_1, x_3, \mathbf{U}_2) &= (\mathbf{u}(x_1, 0, x_3) - \mathbf{u}(x_1, \ell_2, x_3)) - \mathbf{U}_2 = \mathbf{0} \\ \varphi_3(x_1, x_2, \mathbf{U}_3) &= (\mathbf{u}(x_1, x_2, 0) - \mathbf{u}(x_1, x_2, \ell_3)) - \mathbf{U}_3 = \mathbf{0} \end{aligned} \quad (1)$$

86 where $\varphi_{i=1,3}$ are the three constraint equations relating relative displacements
87 $\mathbf{U}_{i=1,3}$ of pair of opposite nodes in the RVE sides. The constraints can be
88 introduced in the discrete potential energy associated to the weak form of
89 the elastic equilibrium problem:

$$\Pi^h(\mathbf{u}^h) = \frac{1}{2} \int_{\Omega^h} \boldsymbol{\sigma}(\mathbf{u}^h) \cdot \nabla \mathbf{u}^h d\Omega - \int_{\Omega^h} \mathbf{u}^h \cdot \mathbf{f} d\Omega - \int_{\partial\Omega^h} \mathbf{u}^h \cdot \mathbf{h} d(\partial\Omega) + \Psi(\mathbf{u}^h) \quad (2)$$

90 where $\boldsymbol{\sigma}(\mathbf{u}^h)$ and $\nabla \mathbf{u}^h$ stands for stress and strain tensors associated to
91 the discrete displacement field \mathbf{u}^h , and \mathbf{f} and \mathbf{h} the body forces and con-
92 tact stresses at the volume and boundary of the solid, respectively. Finally,
93 $\Psi(\mathbf{u}^h)$ represents the potential energy associated to the introduction of the
94 periodicity constraints. In case of explicit time integration, equation 2 can be
95 generalized to the dynamic problem by introducing the inertia and damping
96 forces in the system.

97 The constraint equations (1) can be rearranged to obtain a more appropri-
98 ate form for the FE assembly procedure. For the easy imposition of periodic
99 conditions, the *global* reference nodes (master nodes) M_i and M'_i are defined
100 (figure 1) such that:

$$\mathbf{U}_i = \mathbf{u}_{M_i} - \mathbf{u}_{M'_i} \quad (3)$$

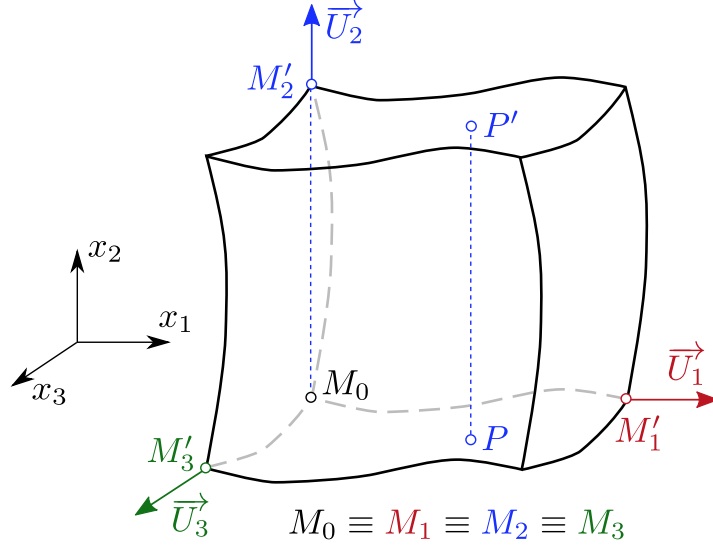


Figure 1: Four nodes involved in the PBC of displacement of nodes P - P' : M_2, M'_2, P, P'

101 The relative motion between a *local* point P belonging to a given plane of
 102 the RVE and point P' on the parallel plane displaced ℓ_i (length of the RVE
 103 in the direction i) can be expressed as the 4-point condition:

$$\varphi_i(\mathbf{u}_P, \mathbf{u}_{P'}, \mathbf{u}_{M_i}, \mathbf{u}_{M'_i}) = (\mathbf{u}_P - \mathbf{u}_{P'}) - (\mathbf{u}_{M_i}, \mathbf{u}_{M'_i}) = \mathbf{0} \quad (4)$$

104 for all pair of opposite nodes P and P' being $\overline{OP'} = \overline{OP} + \ell_i \mathbf{e}_i$, where \mathbf{e}_i
 105 the unit vector perpendicular to the RVE planes. The linear constraint [26]
 106 between the displacements of these four points can be defined as:

$$\begin{aligned}
\boldsymbol{\varphi}^e(\mathbf{u}_P, \mathbf{u}_{P'}, \mathbf{u}_M, \mathbf{u}_{M'}) &= \begin{bmatrix} \varphi_1 \\ \varphi_2 \\ \varphi_3 \end{bmatrix} = \mathbf{L}\mathbf{u}^e = \\
&= \begin{bmatrix} 1 & 0 & 0 & -1 & 0 & 0 & -1 & 0 & 0 & 1 & 0 & 0 \\ 0 & 1 & 0 & 0 & -1 & 0 & 0 & -1 & 0 & 0 & 1 & 0 \\ 0 & 0 & 1 & 0 & 0 & -1 & 0 & 0 & -1 & 0 & 0 & 1 \end{bmatrix} \begin{bmatrix} u_P^1 \\ u_P^2 \\ u_P^3 \\ u_{P'}^1 \\ u_{P'}^2 \\ u_{P'}^3 \\ u_M^1 \\ u_M^2 \\ u_M^3 \\ u_{M'}^1 \\ u_{M'}^2 \\ u_{M'}^3 \end{bmatrix} = \mathbf{0} \quad (5)
\end{aligned}$$

107 Instead of satisfying the constraint exactly, a penalty approach is used
108 such that the deviation from the exact fulfilment of the constraint penalizes
109 the potential energy. If the constraint $\boldsymbol{\varphi}^e = \mathbf{0}$ is verified, the element-wise
110 elastic potential is minimum:

$$\Psi^e(\mathbf{u}^e) = \frac{1}{2}k \boldsymbol{\varphi}^e(\mathbf{u}^e) \cdot \boldsymbol{\varphi}^e(\mathbf{u}^e) = \frac{1}{2}k \mathbf{L}\mathbf{u}^e \cdot \mathbf{L}\mathbf{u}^e \quad (6)$$

111 and the internal forces necessary to obtain a good approximation of the
112 constraints are calculated from the gradient of the potential, according to:

$$\left(\frac{\partial \Psi^e}{\partial \mathbf{u}^e} \right) = k \mathbf{L}^T \mathbf{L}\mathbf{u}^e = \mathbf{F}_k^e \quad (7)$$

113 This approach can be seen as a generalized spring network between nodes
114 belonging to the boundaries, pulling the system back to the periodic con-
115 straint. Hence, its natural implementation in Abaqus/Explicit [25] is by
116 means of 4-node user-defined elements, henceforth named Periodic Bound-
117 ary Condition Elements (PBCE), defined by means of a subroutine VUEL.
118 Each PBCE mimics a local ‘‘penalty’’ constraint between opposite nodes P ,
119 P' , and master nodes M_i , M'_i , as in the system of equations 1. The points
120 $\{M_i, M'_i\}$ are assembled to be the same for each pair of opposite surfaces

121 so that the globally imposed displacement difference \mathbf{U}_i , is the same for all
 122 pairs of opposite nodes P, P' .

123 The *global* constraint $\Psi(\mathbf{u}^h)$ and the external forces \mathbf{F}_{ext} appear natu-
 124 rally when the elements associated with the nodes belonging to the domain
 125 boundaries are assembled, and the displacements/forces are imposed to the
 126 master nodes. The constraint is satisfied approximately for each pair of oppo-
 127 site nodes. With the PBCE, the displacements of nodes M_i are constrained,
 128 whereas the displacements of nodes M'_i are imposed, as in equation 3. It
 129 should be noted that either relative displacements \mathbf{U}_i or forces \mathbf{F}_i can be
 130 externally imposed through the master nodes. For instance, an uniaxial test
 131 in the direction 3 is imposed by means of $\mathbf{U}_3 = (0, 0, \bar{\epsilon}_3 \ell_3)$ and $\mathbf{U}_1 = (u_1, 0, 0)$
 132 and $\mathbf{U}_2 = (0, u_2, 0)$, being $\bar{\epsilon}_3$ the average strain imposed to the RVE in the
 133 direction 3. In this case, u_1 and u_2 stand for the output lateral Poisson
 134 contraction resulting from the FEM computation.

135 As it is presented, this method originates undamped oscillations in dy-
 136 namic analyses, as verified in preliminary simulations. Hence, damping mech-
 137 anisms are implemented in the PBCE while preventing that its valid motions
 138 are affected. Viscous Rayleigh damping gives a force proportional to the neg-
 139 ative rate of change of $\mathbf{L}\dot{\mathbf{u}}^e$ and parallel to the elastic force:

$$\mathbf{F}_c^e = c \mathbf{L}^T \mathbf{L} \dot{\mathbf{u}}^e \quad (8)$$

140 where c is a damping coefficient. For low loading rates, for which the effect of
 141 inertial forces is negligible, an additional mass m can be added to the system
 142 in the same way:

$$\mathbf{F}_m^e = m \mathbf{L}^T \mathbf{L} \ddot{\mathbf{u}}^e \quad (9)$$

143 The resulting equation of motion of the element, taking into account the
 144 external forces, is:

$$\mathbf{0} = \mathbf{F}_k^e + \mathbf{F}_c^e + \mathbf{F}_m^e - \mathbf{F}_{ext}^e = \mathbf{L}^T \mathbf{L} (k\mathbf{u}^e + c\dot{\mathbf{u}}^e + m\ddot{\mathbf{u}}^e) - \mathbf{F}_{ext}^e \quad (10)$$

145 3. Multiscale computational applications

146 The traditional approach to implement PBC is by means of constraint
 147 equations (*EQUATION in Abaqus [25]). This method has strong foundations
 148 for implicit solvers based on static equilibrium, but exhibits several draw-
 149 backs when explicit dynamic time integration (i.e. central differences) is
 150 used. Firstly, the relationships between master and slave displacements is

151 translated into equations that introduce intense high-frequency oscillations
 152 in the system. Secondly, in the specific case of Abaqus/Explicit [25], there is
 153 a limitation in the number of constraint equations supported (around 90000
 154 for Abaqus v6.14 [25]), and no parallel computation is allowed when con-
 155 straint equations involve different element domains. Finally, the method
 156 with traditional PBC is computationally expensive. The Periodic Boundary
 157 Condition Element (PBCE) approach proposed in this paper is more efficient
 158 under similar conditions.

159 In the following, the PBCE method is applied and validated under two
 160 computational homogenization scenarios in composite materials: microme-
 161chanical and mesomechanical homogenization.

162 3.1. Micromechanical homogenization

163 Micromechanical homogenization in composite materials is generally used
 164 to compute the elastic and strength properties of an orthotropic lamina and
 165 predict ply failure envelopes, e.g. [9–11, 15]. The behaviour of the ply trans-
 166 verse to the fibres direction can be analysed with two-dimensional or quasi-2D
 167 RVE, as shown in figure 2. Herewith, a 2D version of the PBCE presented
 168 above is used in the computation of transverse tensile properties of the uni-
 169 directional Carbon-Fibre Reinforced Polymer (CFRP) material AS4/8552.

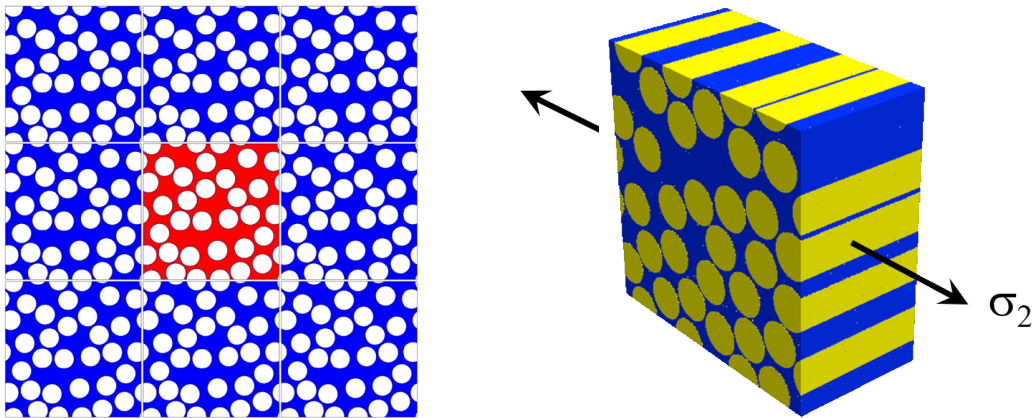


Figure 2: The composite mechanical behaviour is determined by solving numerically the boundary value problem for a RVE of the composite which is much larger than the heterogeneities in the microstructure.

170 The microstructure of the RVE of an unidirectional composite is ideal-
 171 ized as a dispersion of parallel and circular fibres randomly distributed in

172 the polymer matrix. A total of 50 fibres is enough to capture adequately
173 the essential features of the microstructure of the material while maintain-
174 ing reasonable computing efforts, as demonstrated by González and LLorca
175 [27]. Synthetic fibre distributions statistically equivalent to the real ones are
176 generated with a modified Random Sequential Adsorption (RSA) algorithm
177 [12].

178 The RVE is discretized in Abaqus/Explicit [25] in the following way: the
179 matrix and the fibres are modelled with 4-node fully integrated quad isoparam-
180 etric elements under the assumption of plane strain (CPE4), while the fibre-
181 matrix interface debonding is simulated with 4-node cohesive isoparametric
182 elements (COH2D4) inserted at the interfaces between fibres and matrix.
183 Perfect and homogeneous contact between fibres and matrix is assumed. The
184 carbon fibres are assumed to behave as linear elastic transversely isotropic
185 solids. The matrix is modelled as an isotropic elastic-plastic solid accord-
186 ing to a modified Drucker-Prager plasticity yield surface including damage
187 [25, 28]. The fibre-matrix interface behaviour follows a mixed-mode bilinear
188 traction-separation law [25]. More detailed information about the materials
189 constitutive models and properties can be found in [8, 11].

190 A reference analysis was carried out with Abaqus/Standard [25] within
191 the framework of the finite deformations theory. In addition, explicit dy-
192 namic analyses employing the default Abaqus/Explicit [25] PBC scheme, by
193 means of constraint equations, were also run for comparison with the devel-
194 oped PBCE approach. In each analysis, the first thermo-mechanical loading
195 step simulates the cooling-down process from curing to ambient tempera-
196 tures, given the significant influence of the respective residual stresses on the
197 homogenized properties. This step is followed by the application of mechan-
198 ical load up to failure. Two typical load-cases were analysed herein: pure
199 transverse tension and pure transverse compression.

200 A careful selection of the mechanical parameters of the PBCE was done
201 in advance to maximize the accuracy of the simulation without penalizing
202 its computational cost. To this end, the stiffness, k , and damping, c , of the
203 PBCE were estimated to minimize their penalization on the analysis stable
204 time step, Δt_{stab} . A value of damping $c = 0.001 \text{ mN}\mu\text{s}/\mu\text{m}$ was sufficient to
205 remove spurious oscillations, while a stiffness $k = 100 \text{ mN}/\mu\text{m}$ guaranteed
206 the periodicity between opposite edges without penalizing Δt_{stab} . The nodal
207 mass of the PBCE was taken as the average nodal mass of the RVE. For
208 both load cases, the steady-state loading rate selected was $0.1 \mu\text{m}/\mu\text{s}$ with a
209 peak acceleration of $3 \mu\text{m}/\mu\text{s}^2$.

210 The stress-strain curves resulting of the different analyses, as well as stress
211 fields for the tensile cases and strain fields for the compression cases, are
212 shown in figure 3. For transverse tension, it is observed that the mechanical
213 fields are equivalent between implicit and explicit analyses, and that ultimate
214 failure is triggered by the same cracking mechanisms at similar applied stress
215 level (≈ 51.5 MPa) in both schemes. However, the explicit FE results using
216 constraint equations, *EQUATION, are highly oscillatory and under-predict the
217 transverse tensile strength of the material. For transverse compression, the
218 match between implicit and explicit analyses with PBCE is again remarkable
219 in terms of strain fields and load at failure (≈ 205 MPa). The explicit analysis
220 with constraint equations also shows an oscillatory response although the
221 obtained transverse compression strength of the material matches the one
222 predicted by the other two methods.

223 3.2. Mesomechanical homogenization

224 The use of PBC at the mesoscale allows for the definition of a Represent-
225 ative Laminate Element (RLE), in essence a RVE of a laminate [22, 23], as
226 represented in figure 4. The use of PBC aims at introducing an uniform far-
227 field stress to a small portion of the laminated material structure, assuming
228 that the RLE behaviour is statistically representative of the whole specimen
229 [29]. In this way, this approach allows the computation of the homogenized
230 elastic and strength properties for a given laminate configuration in all or-
231 thotropic directions, and the prediction of a laminate failure envelope.

232 The traditional way to determine laminate properties and qualify compos-
233 ite materials for structural applications is through costly and time consuming
234 experimental testing following carefully devised test standards. In the recent
235 years, numerical simulation arose as a promising alternative towards efficient
236 material certification by virtual testing, with the added advantage that a
237 much larger range of configurations can be considered [5, 6, 30]. The standard
238 test methods can be modelled with high-fidelity and accurate predictions of
239 laminate behaviour and relevant properties achieved, as demonstrated by
240 Falcó et al. [24]. Both physical and virtual approaches aim at reproducing a
241 macroscopically homogeneous stress state such that the resultant behaviour
242 can be considered intrinsic to the laminate configuration. However, because
243 of the finite width of the coupons and the three dimensional stress states at
244 their edges [31, 32], the behaviour is significantly affected by edge cracking
245 and delamination. By means of the RLE approach proposed in this paper,
246 edge effects are removed from the boundaries of the numerical model and

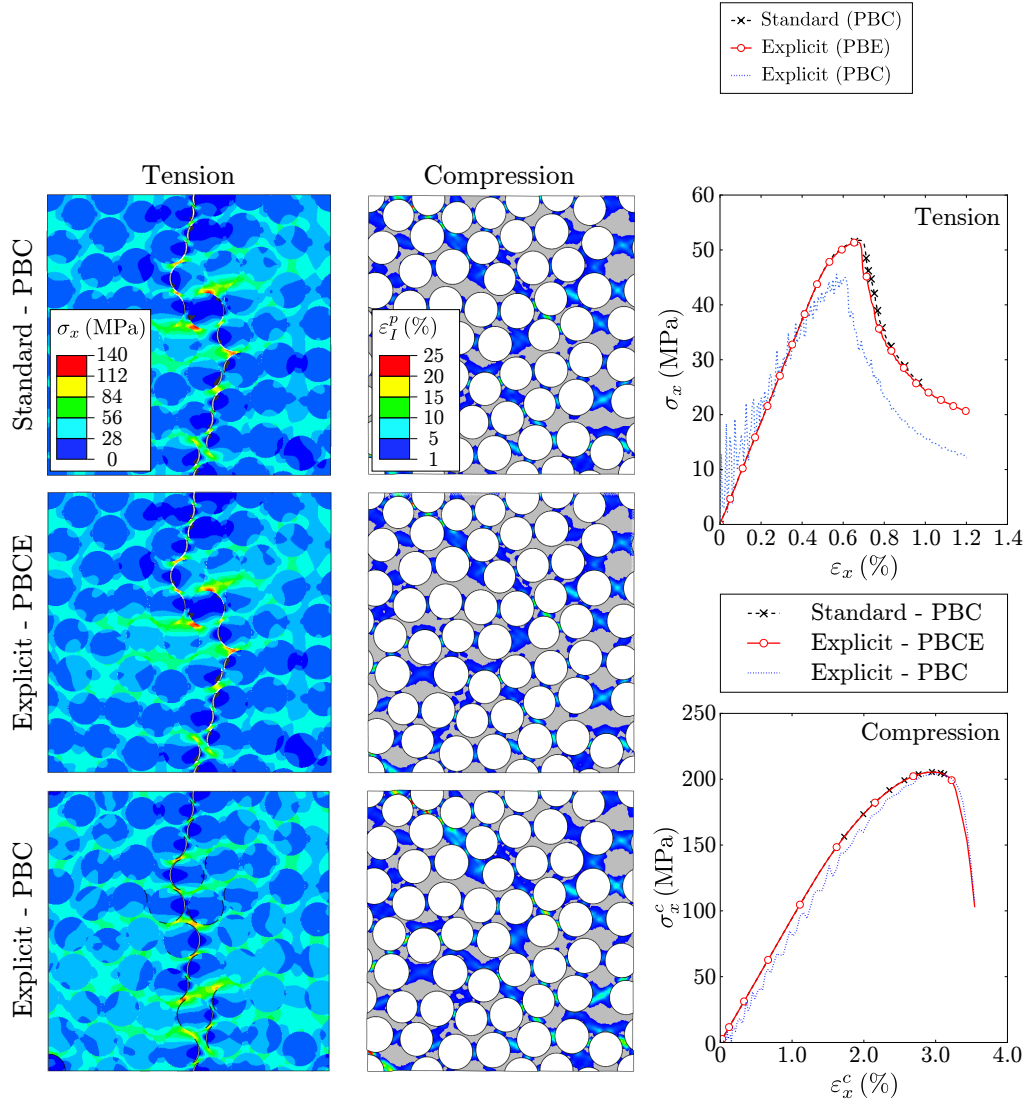


Figure 3: Comparison of the results obtained with Periodic Boundary Conditions Elements (PBCe) in Explicit against the Periodic Boundary Conditions (PBC) in Standard and Explicit by means of constraint equations. Transverse tension (left column) and compression (middle column) load cases are shown. The resulting stress-strain curves for each load case (tension and compression) for the three different schemes are shown in the right column.

247 replaced by PBC, so that the analysis addresses only the material response.
 248 Moreover, the computational requirements are remarkably reduced since the
 249 RLE can be much smaller than the virtual coupon.

250 To capture the relevant mechanisms of laminate behaviour, the RLE do-
 251 main is discretized in plies and ply interfaces. While interlaminar damage is

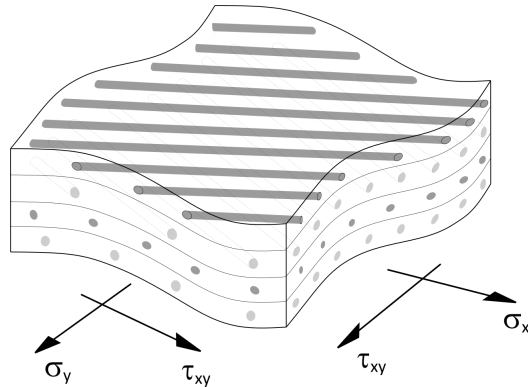


Figure 4: Representative Laminate Element (RLE).

252 assumed to occur in the form of delaminations along predefined and discrete
 253 crack planes, ply damage might occur in the form of fibre breakage, fibre
 254 pull-out, kink-banding and matrix cracking at any location within the plies.
 255 Hence, the appropriate description of the ply interface behaviour is achieved
 256 by means of cohesive and frictional relations between discrete fracture planes
 257 whilst the ply deformation mechanisms can be adequately tackled by means
 258 of a Continuum Damage Model (CDM) [24]. This modelling approach im-
 259 poses severe non-linearities to the numerical problem which are typically
 260 intractable by implicit solvers. Therefore, the explicit numerical integration
 261 of the RLE, coupled with the PBCE proposed in this paper, constitutes the
 262 enabler of the computational homogenization of laminate behaviour.

263 For the purpose of demonstration, the In-Plane Shear (IPS) test on an
 264 AS4-8552 laminate is addressed herein. This experiment is used to charac-
 265 terize the in-plane shear response of a ± 45 laminate, and is defined accord-
 266 ing to the ASTM D3518 test standard [33]. It consists of a rectangular coupon
 267 of $[\pm 45]_s$ configuration, 25 mm in width by up to 250 mm in length, loaded
 268 under quasi-static tension up to failure. To define an appropriate RLE, it
 269 is sufficient to consider an area of $10 \times 10 \text{ mm}^2$ of the laminate, as shown
 270 in figure 5. Since the laminate at any point is statistically representative of
 271 the laminated structure, the only constraint on the dimensions of the RLE
 272 are that it should be much larger than the characteristic dimensions of the
 273 physical mechanisms that are to be simulated. In this case, the relevant
 274 phenomena are matrix cracking and delamination, which are associated to
 275 fracture process zones of the order of less than a millimetre [34]. Moreover,
 276 due to the out-of-plane symmetry of the $[\pm 45]_s$ configuration, only two plies

277 (± 45) need to be modelled with appropriately imposed symmetry boundary
 278 conditions.

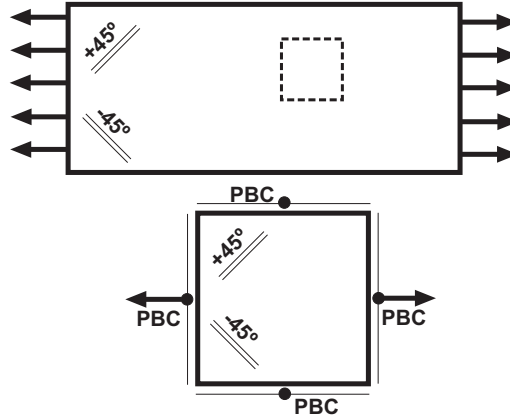


Figure 5: Illustrations of the In-Plane Shear (IPS) test (top) and the corresponding RLE (bottom) with applied PBCs and loads.

279 The laminate modelling approach follows the work of Falcó et al. [24]. Ac-
 280 cordingly, the ply interface response is modelled by means of a general mixed-
 281 mode cohesive zone method coupled with frictional behaviour. The coupled
 282 cohesive-frictional approach is adopted to include the possible effects of ply
 283 friction during and after delamination, and is implemented in the kinematics
 284 of surface contact interaction algorithms available in Abaqus/Explicit [25].
 285 The unidirectional FRP plies are modelled by means of a thermodynamically-
 286 consistent CDM that takes into account the relevant ply deformation mech-
 287 anisms [24]. The nonlinear elastic-plastic shear behaviour of the material
 288 is modelled by a Ramberg-Osgood law [35]. The possibility of elastic un-
 289 loading is tackled by means of a general elastic predictor - plastic corrector
 290 algorithm. The relevant ply and interface properties required by these models
 291 are given in [24]. Similar properties for the same material (different batches)
 292 are available in [36]. A regularized meshing approach is used, with material-
 293 alignment and directional biasing, as described in [24]. Each ply (0.184 mm
 294 in thickness) is discretized with a single through-the-thickness plane of reg-
 295 ular 8-noded hexahedral isoparametric elements of $0.6 \times 0.2 \times 0.184 \text{ mm}^3$
 296 in volume with reduced integration (C3D8R), except around the RLE edges
 297 wherein tetrahedral elements (C3D6R) are used.

298 As in the computational micromechanics case above, a judicious selection
 299 of the mechanical parameters of the PBCE was performed to ensure both

300 the accuracy and the efficiency of the simulation. To this end, the PBCE
 301 damping and stiffness coefficients were set to $c = 0.1 \text{ N s/mm}$ and $k =$
 302 $2 \cdot 10^5 \text{ N/mm}$, respectively. The nodal mass of the PBCE was taken as the
 303 average nodal mass of the RLE.

304 Quasi-static tensile displacements were imposed to the RLE, as repre-
 305 sented in figure 5, until collapse was produced by the accumulation of matrix
 306 cracks and delamination between the $+45^\circ$ and -45° layers. For the purpose
 307 of qualitative correlation (figure 6), the simulated accumulation of matrix
 308 cracks is compared with equivalent experimental results of an IPS test on a
 309 similar carbon/epoxy material which have been obtained by means of X-ray
 310 computed tomography (XCT) [37, 38].

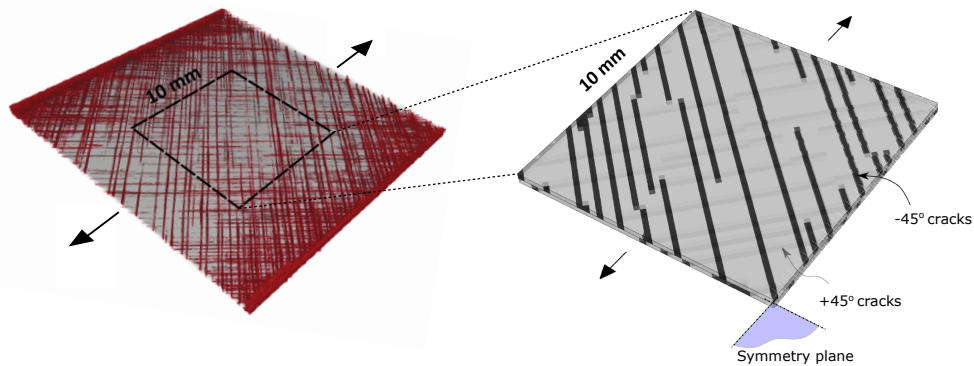


Figure 6: Qualitative correlation between experimentally-obtained (left) and simulated (right) development of matrix cracking in a plain stress $[\pm 45]_s$ laminate (experimental results adapted from [37]). Note: both experiments and simulations performed in similar carbon/epoxy $[\pm 45]_s$ coupons, although not exactly the same material.

311 In the experiments (figure 6, left), cracks develop similarly in the $+45^\circ$
 312 and -45° layers, starting from the edges of the specimen, following directions
 313 parallel to the fibres due to the kinematic constraints imposed by the mi-
 314 crostructure. The crack density is always higher around the edges than in
 315 the specimen central sections and it increases with the applied load until
 316 saturation. Delamination also grows from the specimen edges. Finally, the
 317 accumulation of matrix cracking and delamination leads to instability and
 318 specimen collapse. The simulations on the smaller size RLE (figure 6, right)
 319 capture this damage pattern while discarding the undesirable effects caused
 320 by the edges. It should be mentioned that, whilst the XCT is able to capture
 321 critical and sub-critical damage mechanisms, the simulations only predict the

322 first, i.e. cracks completely developed through the thickness of the plies. Al-
323 though the CDM does not contain information of the kinematic constraints
324 imposed by the ply microstructure (the shear parallel and perpendicular to
325 the fibre are represented with the same deformation tensor), this effect is ob-
326 tained with the regularized meshing with material-alignment and directional
327 biasing [24], leading to the correct simulation of crack directions. Hence, the
328 RLE can be considered approximately representative of the central sections
329 of the finite-width IPS coupon.

330 The results of the simulation in terms of the stress-strain curve are shown
331 in figure 7. The behaviour of the RLE is nonlinear in a very similar way to the
332 Ramberg-Osgood law [35] implemented at the constitutive level to describe
333 the pure shear stress vs. shear strain relation of the ply, although not exactly
334 since the IPS test configuration does not create pure shear on the ply but
335 a mixed-mode loading situation, with a small fraction of transverse tension.
336 For this same reason, the ultimate IPS load, $IPSS = 99.7$ MPa, also diverges
337 from the ply shear strength, $S_L = 110.4$ MPa [36]. This demonstrates that
338 this property is not adequately characterized by the IPS experiment [33],
339 and a better alternative for that purpose is the Short Beam test standard
340 ASTM D2344M [39] that measures the Interlaminar Shear Strength (ILSS)
341 in a laminate.

342 Through-the-thickness matrix cracking, as shown in figure 6, initiates at
343 the highest load and deformation stages, rapidly growing and interacting with
344 interface delamination to produce the collapse of the RLE. The simulated
345 cracking is, however, not influenced by coupon edge effects as in the IPS
346 experiment. As result, the numerically obtained In-Plane Shear Strength,
347 $IPSS = 99.7$ MPa is higher than the average value obtained experimentally
348 with the IPS experiment, $IPSS = 91.56$ MPa [36].

349 The numerically-obtained unloading-reloading behaviour of the RLE is
350 also represented in figure 7 to demonstrate that the PBCE, and the consti-
351 tutive ply model, work well under these circumstances.

352 4. Conclusion

353 Special-purpose Periodic Boundary Elements (PBCE) were proposed to
354 impose Periodic Boundary Conditions (PBC) to general Representative Vol-
355 ume Elements (RVE) in FE solvers with dynamic explicit time integration.
356 This approach solves the issue of spurious displacement oscillations resulting

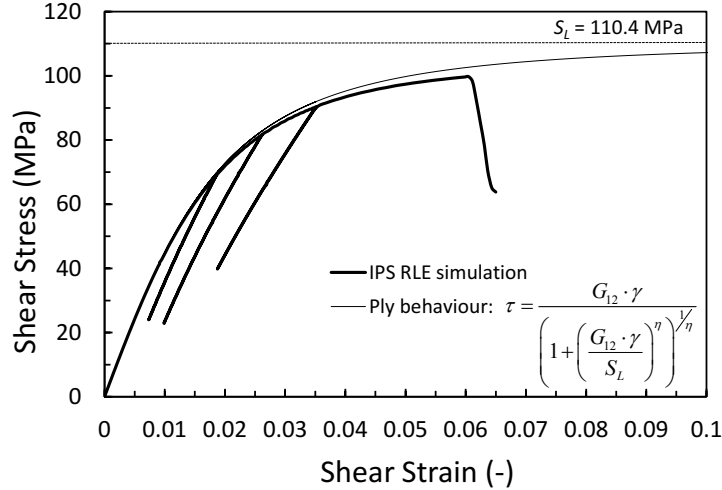


Figure 7: Stress-strain curves for the plain tension test. The appearance of the relevant damage events are marked with arrows in the figure. Ply in-plane shear strength, $S_L = 110.4$ MPa, measured by means of the Short Beam Test [36]. Numerically-obtained laminate In-Plane Shear Strength, IPSS = 99.7 MPa (at $\gamma_{pl} = 0.04\%$). Experimentally-obtained $[\pm 45]_s$ specimen IPSS = 91.6 MPa (SD = 2.51 MPa) corresponding to $\gamma_{pl} = 0.05$ [36]. Ply in-plane shear modulus $G_{12} = 4.9$ GPa. Ramberg-Osgood exponential, $\eta = 1.9$.

357 from the application of traditional PBC in explicit FE. The PBCE formu-
 358 lation was implemented by means of a user-defined element through a VUEL
 359 subroutine in Abaqus/Explicit [25]. The reliability and applicability of the
 360 approach were demonstrated in the framework of multiscale computational
 361 analysis of composites. First, the PBCE method in combination with RVEs
 362 were applied to micromechanical homogenization of unidirectional FRP yarns
 363 or plies. The correlation between traditional PBC in implicit integration and
 364 PBCE in explicit FE was remarkable. Then, PBCE in combination with Rep-
 365 resentative Laminate Elements (RLE) were proposed for the homogenization
 366 of laminate behaviour through computational mesomechanics to expedite
 367 the virtual testing of composite materials and eliminate undesired effects of
 368 coupon-based experiments.

369 Acknowledgements

370 The research leading to this publication was supported by the European
 371 Community FP7 Programme through project MAAXIMUS (grant agreement
 372 213371) and by the Spanish Ministry of Industry, Economy and Competi-

373 tiveness (MINECO) through project HYDTCOMP (grant MAT2015-69491-
374 C03-02). C.S. Lopes also acknowledges the support of MINECO through the
375 *Ramón y Cajal* fellowship (grant RYC-2013-14271). The authors are grateful
376 to Prof. Ignacio Romero for his helpful insights on this research.

377 References

- 378 [1] T. Kanit, S. Forest, I. Galliet, V. Mounoury, D. Jeulin, Determination
379 of the size of the representative volume element for random composites:
380 Statistical and numerical approach, *International Journal of Solids and*
381 *Structures* 40 (2003) 3647–3679.
- 382 [2] V. D. Nguyen, E. Béchet, C. Geuzaine, L. Noels, Imposing periodic
383 boundary condition on arbitrary meshes by polynomial interpolation,
384 *Computational Materials Science* 55 (2012) 390–406.
- 385 [3] J. M. Tyrus, M. Gosz, E. DeSantiago, A local finite element imple-
386 mentation for imposing periodic boundary conditions on composite mi-
387 cro-mechanical models, *International Journal of Solids and Structures*
388 44 (2007) 2972–2989.
- 389 [4] F. J. P. Reis, F. M. Andrade Pires, A mortar based approach for the
390 enforcement of periodic boundary conditions on arbitrarily generated
391 meshes, *Computer Methods in Applied Mechanics and Engineering* 274
392 (2014) 168–191.
- 393 [5] C. S. Lopes, C. González, O. Falcó, F. Naya, J. Llorca, B. Tijs, Multi-
394 scale virtual testing: the roadmap to efficient design of composites for
395 damage resistance and tolerance, *CEAS Aeronautical Journal* 7 (2016)
396 607–619.
- 397 [6] J. Llorca, C. González, J. M. Molina-Aldareguía, J. Segurado, R. Seltzer,
398 F. Sket, M. Rodríguez, S. Sádaba, R. Muñoz, L. P. Canal, Multiscale
399 modeling of composite materials: a roadmap towards virtual testing.,
400 *Advanced materials* 23 (2011) 5130–47.
- 401 [7] J. Llorca, C. González, J. Molina-Aldareguía, C. Lopes, Multiscale mod-
402 eling of composites: Toward virtual testing... and beyond, *The Journal*
403 *of The Minerals, Metals & Materials Society (TMS)* 65 (2013) 215–225.

- 404 [8] M. Herráez, C. González, C. Lopes, R. G. de Villoria, J. LLorca,
405 T. Varela, J. Sánchez, Computational micromechanics evaluation of the
406 effect of fibre shape on the transverse strength of unidirectional com-
407 posites: An approach to virtual materials design, *Composites Part A:
408 Applied Science and Manufacturing* 91 (2016) 484–492.
- 409 [9] A. Melro, P. Camanho, F. Andrade Pires, S. Pinho, Micromechani-
410 cal analysis of polymer composites reinforced by unidirectional fibres:
411 Part II Micromechanical analyses, *International Journal of Solids and
412 Structures* 50 (2013) 1906–1915.
- 413 [10] T. Vaughan, C. McCarthy, A micromechanical study on the effect of
414 intra-ply properties on transverse shear fracture in fibre reinforced com-
415 posites, *Composites Part A: Applied Science and Manufacturing* 42
416 (2011) 1217–1228.
- 417 [11] F. Naya, C. González, C. S. Lopes, S. V. der Veen, F. Pons, Computa-
418 tional micromechanics of the transverse and shear behavior of unidirec-
419 tional fiber reinforced polymers including environmental effects, *Com-
420 posites Part A: Applied Science and Manufacturing* 92 (2017) 146–157.
- 421 [12] J. Segurado, J. Llorca, A numerical approximation to the elastic prop-
422 erties of sphere-reinforced composites, *Journal of the Mechanics and
423 Physics of Solids* 50 (2002) 2107–2121.
- 424 [13] J. Williams, J. Segurado, J. LLorca, N. Chawla, Three dimensional
425 (3D) microstructure-based modeling of interfacial decohesion in particle
426 reinforced metal matrix composites, *Materials Science and Engineering:
427 A* 557 (2012) 113–118.
- 428 [14] O. Pierard, C. González, J. Segurado, J. LLorca, I. Doghri, Microme-
429 chanics of elasto-plastic materials reinforced with ellipsoidal inclusions,
430 *International Journal of Solids and Structures* 44 (2007) 6945–6962.
- 431 [15] F. Naya, M. Herráez, C. S. Lopes, C. González, S. V. der Veen, F. Pons,
432 Computational micromechanics of fiber kinking in unidirectional FRP
433 under different environmental conditions, *Composites Science and Tech-
434 nology* 144 (2017) 26 – 35.

- 435 [16] M. Herráez, A. Fernández, C. Lopes, C. González, Strength and tough-
436 ness of structural fibres for composite material reinforcement, *Philos-*
437 *ophical Transactions of the Royal Society A* 374 (2016) 1–11.
- 438 [17] F. Naya, J. M. Molina-Aldareguía, C. Lopes, C. González, J. Llorca, In-
439 terface characterization in fiber-reinforced polymer-matrix composites,
440 *The Journal of The Minerals, Metals & Materials Society (TMS)* 69
441 (2017) 13–21.
- 442 [18] A. R. Melro, P. P. Camanho, F. M. Andrade Pires, S. T. Pinho, Numer-
443 ical simulation of the non-linear deformation of 5-harness satin weaves,
444 *Computational Materials Science* 61 (2012) 116–126.
- 445 [19] C. Zhang, W. K. Binienda, R. K. Goldberg, L. W. Kohlman, Meso-scale
446 failure modeling of single layer triaxial braided composite using finite el-
447 ement method, *Composites Part A: Applied Science and Manufacturing*
448 58 (2014) 36–46.
- 449 [20] G. Anzelotti, G. Nicoletto, E. Riva, Mesomechanic strain analysis
450 of twill-weave composite lamina under unidirectional in-plane tension,
451 *Composites Part A: Applied Science and Manufacturing* 39 (2008) 1294–
452 1301.
- 453 [21] A. García-Carpintero, M. Herráez, J. Xu, C. S. Lopes, C. González,
454 A Multi Material Shell Model for the Mechanical Analysis of Triaxial
455 Braided Composites, *Applied Composite Materials* 24 (2017) 1425–1445.
- 456 [22] Z. Xia, Y. Zhang, F. Ellyin, A unified periodical boundary conditions
457 for representative volume elements of composites and applications, *In-*
458 *ternational Journal of Solids and Structures* 40 (2003) 1907–1921.
- 459 [23] Y. Zhang, Z. Xia, F. Ellyin, Two-scale analysis of a filament-wound
460 cylindrical structure and application of periodic boundary conditions,
461 *International Journal of Solids and Structures* 45 (2008) 5322–5336.
- 462 [24] O. Falcó, R. L. Ávila, B. Tijs, C. S. Lopes, Modelling and simulation
463 methodology for unidirectional composite laminates in a virtual test lab
464 framework, *Composite Structures* 190 (2018) 137159.
- 465 [25] Abaqus version 6.14 online documentation, Analysis user’s manual,
466 Simulia Inc., Dassault Systèmes, 2013.

- 467 [26] R. E. Bridson, CPSC 426 computer animation, Department
468 of Computer Science, University of British Columbia,
469 www.cs.ubc.ca/~rbridson/courses/533b-winter-2004/cs533b_slides_jan27.pdf,
470 2004.
- 471 [27] C. González, J. LLorca, Mechanical behavior of unidirectional fiber-
472 reinforced polymers under transverse compression: Microscopic mech-
473 anisms and modeling, *Composites Science and Technology* 67 (2007)
474 2795–2806.
- 475 [28] D. C. Drucker, W. Prager, Soil mechanics and plastic analysis for limit
476 design, *Quarterly of Applied Mathematics* 10 (1952) 157–165.
- 477 [29] J. Segurado, J. LLorca, A numerical approximation to the elastic prop-
478 erties of sphere-reinforced composites, *Journal of the Mechanics and*
479 *Physics of Solids* 50 (2002) 2107 – 2121.
- 480 [30] J. LLorca, C. González, J. Molina-Aldareguía, C. López, Multiscale
481 modeling of composites: Toward virtual testing... and beyond, *JOM* 65
482 (2013) 215–225.
- 483 [31] R. B. Pipes, N. Pagano, Interlaminar stresses in composite laminates
484 under uniform axial extension, *Journal of Composite Materials* 4 (1970)
485 538–548.
- 486 [32] C. Mittelstedt, W. Becker, The pipes–pagano-problem revisited: Elastic
487 fields in boundary layers of plane laminated specimens under combined
488 thermomechanical load, *Composite Structures* 80 (2007) 373 – 395.
- 489 [33] ASTM, Standard test method for in-plane shear response of polymer
490 matrix composite materials by test of a $\pm 45^\circ$ laminate, Technical Re-
491 port, American Society for Testing and Materials (ASTM), West Con-
492 shohocken, PA, USA, 1994. ASTM D3518/3518M-94.
- 493 [34] A. Turon, P. Camanho, J. Costa, C. Dávila, A damage model for the
494 simulation of delamination in advanced composites under variable-mode
495 loading, *Mechanics of Materials* 38 (2006) 1072–1089.
- 496 [35] W. Ramberg, W. R. Osgood, Description of stress-strain curves by three
497 parameters, National Advisory Committee For Aeronautics (1943).
498 Technical Note No. 902.

- 499 [36] NCAMP, Hexcel 8552 AS4 Unidirectional Prepeg Qualification Stati-
500 cal Analysis Report, Technical Report, National Center for Advanced
501 Materials Performance, 2011. CAM-RP-2010-002 May 6, Revision A.
- 502 [37] F. Sket, A. Enfedaque, C. Alton, C. D. Gonzalez, J. M. Molina-
503 Aldareguia, J. LLorca, Automatic quantification of matrix cracking
504 and fiber rotation by x-ray computed tomography in shear-deformed
505 carbon fiber-reinforced laminates., *Composites Science and Technology*
506 90 (2014) 129–138.
- 507 [38] F. Sket, M. Rodríguez-Hortalá, J. Molina-Aldareguía, J. Llorca,
508 E. Maire, G. Requena, In situ tomographic investigation of damage
509 development in $\pm 45^\circ$ carbon fibre reinforced laminates, *Materials Sci-*
510 *ence and Technology* 31 (2015) 587–593.
- 511 [39] ASTM, Standard Test Method for Short-Beam Strength of Polymer Ma-
512 trix Composite Materials and Their Laminates, Technical Report, Amer-
513 ican Society for Testing and Materials (ASTM), West Conshohocken,
514 PA, USA, 2000. ASTM D 2344-2344M(2000).